Journal of Material Cycles and Waste Management (2022) 24:2015–2029
https://doi.org/10.1007/s10163-022-01461-2

ORIGINAL ARTICLE

Study on the kinetics of the conversion of Moroccan phosphogypsum into X_2SO_4 (X = Na, NH_4)

Khalid Agayr[1,2] · Hamza Chanouri[1,2] · Brahim Achiou[3] · Rachid Benhida[1,2] · Khaoula Khaless[1]

Received: 26 February 2022 / Accepted: 30 June 2022 / Published online: 21 July 2022
© Springer Japan KK, part of Springer Nature 2022

Abstract

Phosphoric acid production industries use the wet process, which leads to enormous quantities of phosphogypsum (PG) as a byproduct. The discharge of PG into the oceans is currently considered to be a serious and global issue not only because of environmental damage but also due to economic sulfur loss. In this study, a process of phosphogypsum (PG) conversion was investigated using sodium carbonate (Na_2CO_3) and ammonium bicarbonate (NH_4HCO_3). A kinetic study of the conversion was assessed by shrinking-core models (SCMs). The mixed model was proven to be an effective model that fits the experimental data for the conversion using both reagents well. The results reveal that the conversion is controlled by both interfacial reaction and diffusion through the product layer of PG particles. The optimum conversion rate of PG into Na_2SO_4 was found to be 96–98%. Meanwhile, $(NH_4)_2SO_4$ was obtained from PG with a conversion rate of 96%. This study definitively gives the optimal limitation of two conversion processes, which shows that conversion using sodium carbonate has a good benefit for PG treatment.

Graphical abstract

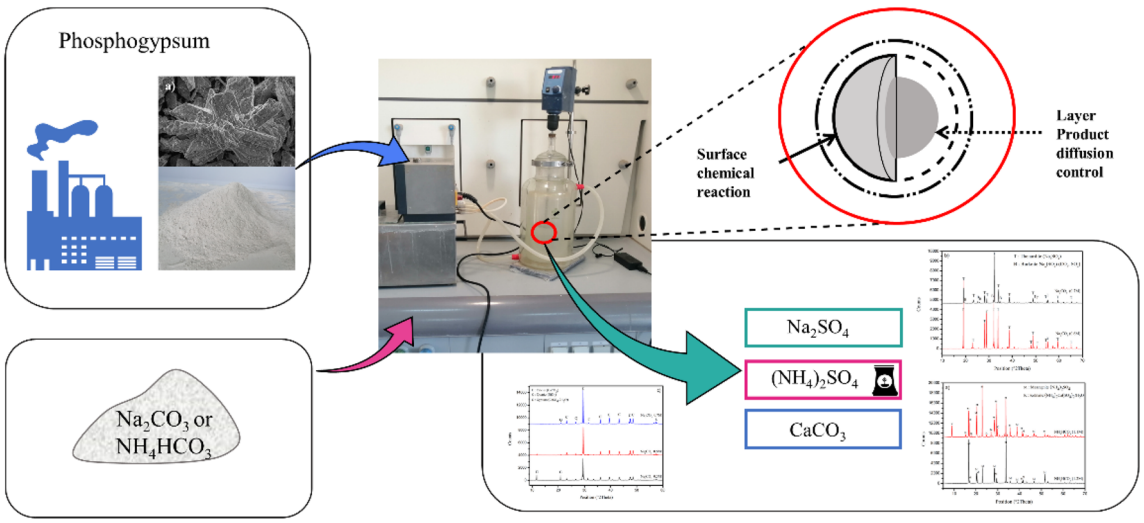

Keywords Phosphogypsum · Sulfate recovery · Shrinking-core model · Calcium carbonate

Introduction

Phosphogypsum (PG) is a byproduct of phosphoric acid production industries generated from a wet process phosphoric acid (WPPA), with particle sizes generally ranging

✉ Khaoula Khaless
Khaoula.KHALESS@um6p.ma

Extended author information available on the last page of the article

from 0.01 to 1 mm [1]. PG mainly consists of gypsum ($CaSO_4.2H_2O$), and contains some impurities such as silica (SiO_2), phosphate, aluminum oxide, and heavy metals [2]. The WPPA is economic, but it generates a large amount of waste. The production of 1 ton of phosphoric acid generates approximately 3–5 tons of PG [3]. Morocco is one of the leaders of the phosphate and phosphoric acid industry in the world. The Moroccan Phosphates Board (OCP group) generates approximately 15 Mt of PG each year [4], and the annual production of PG worldwide is estimated to be 100–250 Mt [5]. However, 85% of this byproduct is usually disposed of into oceans or generally dumped in large stockpiles without any treatment [6]. The storage of PG causes environmental and human health problems due to the release of contaminants such as radionuclides in surface and underground water [7]. Corisco et al. confirmed the accumulation of heavy metals and radionuclides in *Bryum sp.* and *Plantago sp*. tissues growing naturally on PG piles [6]. The accumulation of cadmium in both plant tissues and edible parts has also been reported [8]. Therefore, there is an urgent need to develop a valorization process for this byproduct. Recently, different studies have attempted to valorize PG stockpiles in building materials that seems to be the largest field, such as brick cement or plasterboard [9].

Fig. 1 WPG dried and milled

In agriculture, PG is used as a source of calcium and sulfate for soil amendment [10, 11], or to extract valuable elements such as V, U, I_2 and rare-earth elements [12, 13]. Moreover, it has also been used for the stabilization of bauxite residue [14]. Many researchers have studied the dissolution of PG in different areas including distilled water, seawater, and salt solutions [15]. Others have tried thermal decomposition in the presence of a solid fuel (coal or shale) to produce sulfur dioxide SO_2 and the calcium oxide CaO [16]. However, the decomposition process requires high energy and generates toxic and corrosive gases such as CO, CO_2, and SO_2. For these reasons, researchers have focused on the conversion of PG under less-aggressive conditions. Ennaciri et al. transformed PG into lithium sulfate (Li_2SO_4) at 25 °C, using lithium carbonate (Li_2CO_3) with a concentration of 0.3 M [4]. Agli et al. produced potassium sulfate from PG using potassium chloride (KCl) at a concentration of 1,74 M [17]. Zemni et al. used sodium silicate (Na_2SiO_3) even with its high price to precipitate calcium ions [18].

The conversion of PG is also carried out by carbonation (CO_2 bubbling) after dissolving PG in NaOH solution [19], and ammonia and CO_2 have also been used [20]. The precipitation reaction of calcium in an aqueous system using carbonate reagent offers a high economic potential in the reuse of PG compared to other precipitation reagents such as NaOH, Na_2SiO_2, and KOH due to their high cost. Thus, in this study, the use of low-cost reagents was proposed. $(NH_4)_2CO_3$ has been used in several studies to produce $(NH_4)_2SO_4$ which can be used as a fertilizer (the Merseburg process) [21]. The kinetic parameters of the reaction process were estimated by Danielik et al. using a mathematical model. They found that the reaction proceeded in the liquid phase and not at the surface of the solid particles [22]. Kandil et al. obtained highly purified $(NH_4)_2SO_4$ using the same process with an additional step of purification using sulfuric acid before conversion [23]. Sodium sulfate was also formed by reacting PG with sodium carbonate without further kinetic information. Mulopo et al. found that the conversion of PG into $CaCO_3$ reached 98.5% after 105 min using a Na_2CO_3/PG molar ratio of 2 and slurry concentration of 5% [24]. Sodium sulfate has several applications such as

Table 1 Factors and levels of PG conversion experiments using sodium carbonate (X1) and using ammonium bicarbonate (X2)

Effect	PG	Mass	Concentration (M)	Temperature (°C)	L/S ratio	Time (min)
Concentration	X1	100	0.20–0.80	22	10	60
	X2	100	0.50–1.40	22	10	90
L/S ratio	X1	100	0.40–0.85	22	7–15	60
	X2	100	0.97–1.53	22	7–15	90
Time	X1	100	0.60	22	10	2–120
	X2	100	1.2	22	10	10–120
Temperature	X1	200	1.19	27–90	5	60
	X2	200	2.33	24–80	5	90

the manufacture of detergents, the kraft process (papermaking), glass, and textile. The precipitated $CaCO_3$ obtained from PG could be used in different areas such as in remediation of acid mine drainage to control wastes acidity [24], paper production, construction, and cement manufacturing [25, 26]. The phosphate industry can use this precipitate for flue-gas desulfurization or in other applications such as the recovery of radionuclides and rare-earth elements (REEs) [12]. In addition to the benefits derived from the production of Na_2SO_4, $(NH_4)_2SO_4$, and $CaCO_3$, the mineral carbonation process has more environmental benefits considering effective industrial waste management. Based on the conversion rate of PG, different models have been tested. The shrinking-core models (SCMs) describe how PG particles are converted into calcium carbonate, by determining the slowest step that controls the conversion reaction of PG [27–29].

This present work aims to investigate the conversion of PG using Na_2CO_3 and NH_4HCO_3 reagents. The effect of each of the following parameters including concentration, L/S ratio, contact time, and temperature on the conversion rate of PG was also studied. Shrinking-core models were applied to understand the kinetic mechanism of the conversion. Then, the economic feasibility of the conversion processes was discussed to develop an efficient process for the valorization of PG.

Materials and methods

Materials

The PG used in this study was provided by the OCP group (Moroccan fertilizer company), Jorf Lasfar, El Jadida, Morocco. Sodium carbonate (Na_2CO_3, 98.5 wt%) was supplied by Soda Solvay and ammonium bicarbonate (NH_4HCO_3, food grade) was provided by Weifang Zhenxing Coking CO., Ltd. Analytical reagent grade barium chloride ($BaCl_2$, > 99 wt%) was purchased from Aromatic Chemicals-GB. It should be mentioned that the water used for all experiments was distilled water.

Conversion of PG

PG contains soluble and insoluble impurities that should be removed. PG purification was first performed by washing with distilled water to remove impurities prior to conversion. The L/S weight ratio of PG washing is 2. The mixture was stirred for 15 min at room temperature to remove impurities such as residual acids and organic matter [30]. The washed PG was dried overnight in the oven at 60 °C and crushed (Fig. 1). Then, PG was added to the reagent solution under vigorous stirring. The obtained slurry was filtered using filter paper (PRAT DUMAS). The precipitate was dried in an oven at 60 °C for 24 h. The filtrate was evaporated at 120 °C to form Na_2SO_4 and $(NH_4)_2SO_4$ depending on the reagent solution used to convert washed phosphogypsum (WPG). The experimental factors and their levels are listed in (Table 1).

The general process consists of the conversion of calcium sulfate dihydrate present in phosphogypsum in aqueous medium. Calcium and sulfate ions combine by ion exchange with the appropriate reagent ions. Calcium ions precipitate in the form of $CaCO_3$ and sulfates are released in the filtrate depending on the reagent used. However, PG was converted in the first process by sodium carbonate according to the reaction Eq. (1)

$$Na_2CO_3(aq) + CaSO_4.2H_2O(s) \rightarrow Na_2SO_4(aq) + CaCO_3(s) + 2H_2O(l) \quad (1)$$

Table 2 Chemical composition of PG (Jorf lasfar)

Major elements	Wt %	Trace elements	mg/kg	Trace elements	mg/kg
SO_3	44.7	Y	152	Dy	10.12
CaO	32.9	La	87.7	Ho	4.3
SiO_2	2.66	Ce	53.46	Er	7.19
Na_2O	0.15	Nd	56.25	Tm	1.74
Fe_2O_3	0.04	Sc	9.91	Yb	5.54
Al_2O_3	0.16	Pr	16.1	Lu	1.55
P_2O_5	0.9	Sm	7.84	V	9
MgO	0.02	Eu	3.39	Cd	< 2
F	1.88	Gd	12.86	As	< 1
K_2O	0.01	Tb	3.05		

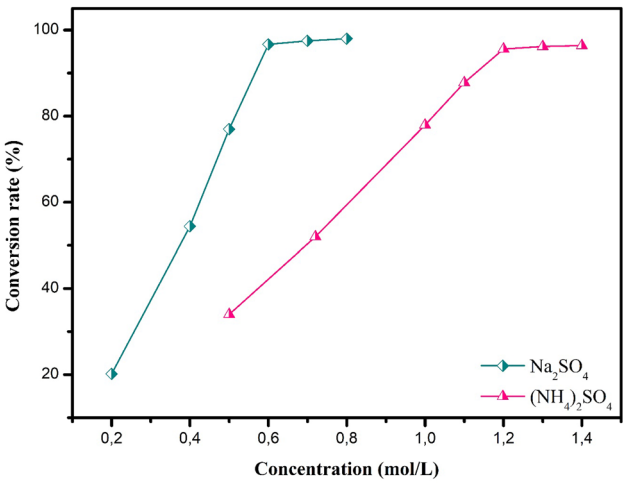

Fig. 2 Effect of sodium carbonate and ammonium bicarbonate concentration on the conversion rate of PG

The second process consists of the use of ammonium bicarbonate to convert PG according to the chemical reaction Eq. (2)

$$2NH_4HCO_3(aq) + CaSO_4.2H_2O(s) \rightarrow (NH_4)_2SO_4(aq) + CaCO_3(s) + CO_2(g) + 3H_2O(l) \quad (2)$$

Since the solubility product of $CaCO_3$ ($Ks = 3.3 \times 10^{-9}$ at 25 °C) is less than that of gypsum ($Ks = 3.14 \times 10^{-5}$ at 25 °C), the reactions in Eq. (1) and Eq. (2) move toward the direction of $CaCO_3$ precipitation and the formation of Na_2SO_4 and $(NH_4)_2SO_4$ products. The conversion rate of PG was determined by Eq. (3)

$$Conversion = m\left(SO_4^{2-}\right)_F / m\left(SO_4^{2-}\right)_{PG} \times 100 \quad (3)$$

Where $m(SO_4^{2-})_{PG}$ is the mass of SO_4^{2-} in PG and $m(SO_4^{2-})_F$ is the mass of SO_4^{2-} in the filtrate.

Characterization techniques

The analysis of crystalline phases was carried out with X-ray diffraction (XRD) D8 Advance Bruker, *CuKα (1.5418 Å)* radiation with a scan 2θ ranging from 5 to 70°. Data analysis phases were conducted using X'Pert High Score Plus software. The morphology was observed using scanning electron microscopy (SEM), FEI ESEM Quanta 450 FEG, and Fourier transform infrared spectroscopy (FTIR) using a JASCO 4600 spectrometer. The FTIR spectra were recorded in the region of 4000–400 cm^{-1} with a resolution of 4 cm^{-1}.

Analytical techniques

pH was measured by a multiparameter WTW model 3630IDS. The sulfate concentration was measured by the gravimetric method according to the Indian Standard IS 3025. It involves the precipitation of barium sulfate ($BaSO_4$) by the addition of barium chloride solution. The calcium concentration was determined by titration of excess ethylene glycol-bis (2-aminoethyl ether)-N, N, N′, N′-tetraacetic acid (EGTA) using calcium carbonate solution. The analysis of the major, minor, and trace elements was carried out using Inductively Coupled Plasma Optical Emission Spectroscopy (ICP–OES) Thermo Jarrell Ash IRIS Advantage and (ICP–MS) Perkin Elmer Nexion® 300X, and the samples to be analyzed are prepared in advance by a total dissolution of 1 g of sample in perchloric acid under 250 °C, and then, a filtration step was performed.

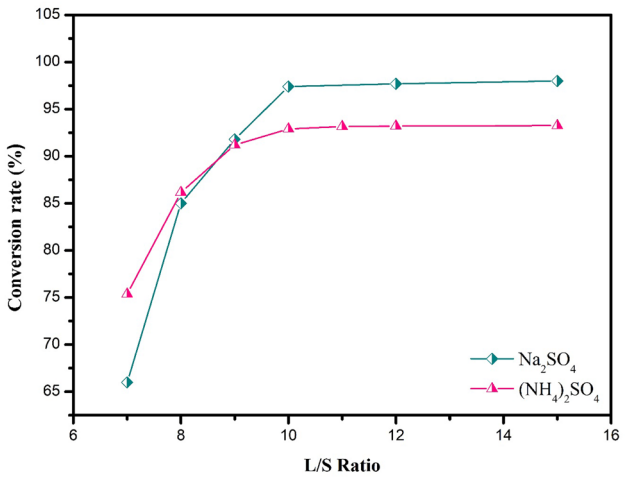

Fig. 3 Effect of the L/S ratio on the PG conversion rate using sodium carbonate and ammonium bicarbonate

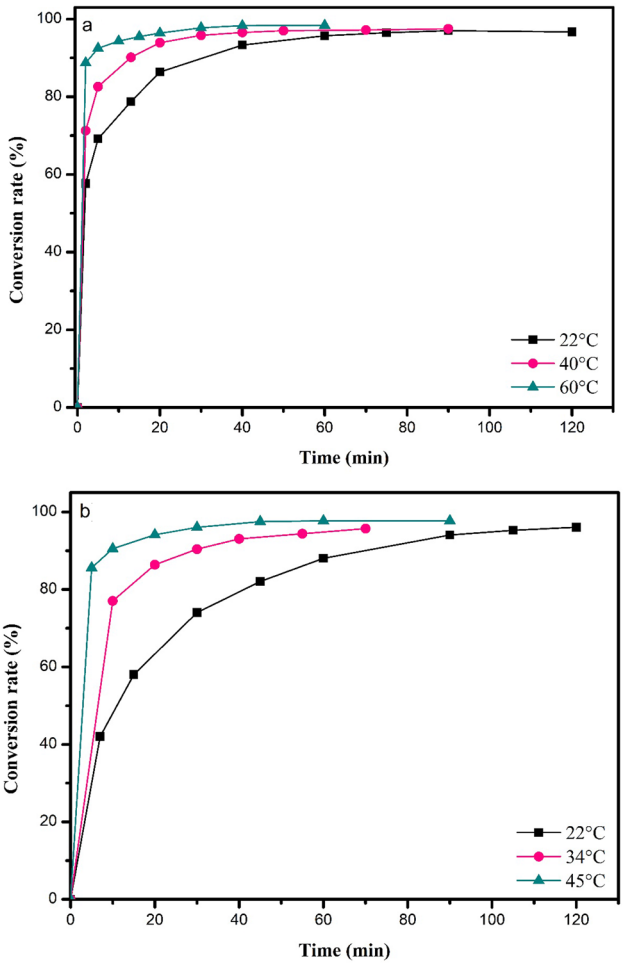

Fig. 4 Effect of reaction time on PG conversion rate using **a** sodium carbonate and **b** ammonium bicarbonate

Results and discussion

PG treatment

The chemical composition of PG depends on several parameters, such as the origin of phosphate rock and the transformation process, which affects its purity, solubility, and conversion. Therefore, PG was washed with distilled water to reduce impurities. Moroccan PG is typically a gray-colored material mainly composed of dehydrated calcium sulfate ($CaSO_4.2H_2O$), PG has a fine grain size, and the crystals are tabular in shape and range in length from 40 to 200 µm, with percentages of 38, 42 and 19% for a median length of about 40, 120 and 200 µm respectively. Table 2 presents the chemical composition of PG. The initial pH (5 wt% slurry) of raw PG is 3.4. The acidic character of PG is due to the presence of water-soluble fluorinated compounds (H_2SiF_6, Na_2SiF_6, K_2SiF_6, and HF), traces of unwashed phosphoric and sulfuric acid and phosphoric salts [31]. After five cycles of washing, it was observed that the pH of PG increased to 5.1 which means that a part of the soluble acids was removed.

PG conversion

Concentration effect

The concentration effects of Na_2CO_3 and NH_4HCO_3 on the conversion of PG were studied to optimize the process. Figure 2 illustrates the conversion rate of PG at ambient temperature (22 °C) as a function of the concentration of Na_2CO_3 in the range of 0.2–0.8 M with a L/S Ratio of 10 at 60 min. As clearly seen, the conversion rate linearly increases with the concentration in the range of 0.2 to 0.6 M to reach the maximum value of 96.7%. The amount of 3.3% that could not be extracted is due to the insoluble sulfates which are complexed with other impurities such as radium and REEs. Moreira et al. used this property to remove radium and thorium from PG based on the difference in solubility, and radium sulfate ($Ks = 3.66 \times 10^{-11}$) is less soluble than calcium sulfate ($Ks = 3.14 \times 10^{-5}$) [32]. When the concentration exceeded 0.6 M, the conversion rate remains constant, since the PG in the solution is totally consumed. Therefore, it can be revealed that the optimum concentration is 0.6 M, which is equivalent to the stoichiometric conditions.

The same variation behavior of the conversion as a function of the concentration (0.5–1.4 M of NH_4HCO_3 was obtained (Fig. 2). The conversion efficiency proportionally increased with concentration in the range of 0.5 to 1.2 M. As clearly seen, the maximum conversion value was found to be 95.6% at 1.2 M. For concentrations beyond 1.2 M, the conversion rate remained steady at 96.6%, indicating that the optimal concentration was 1.2 M, which is equivalent to a 3.3% excess of NH_4HCO_3. Therefore, in the next experiments, the amount of NH_4HCO_3 was fixed at 3.3% of the excess.

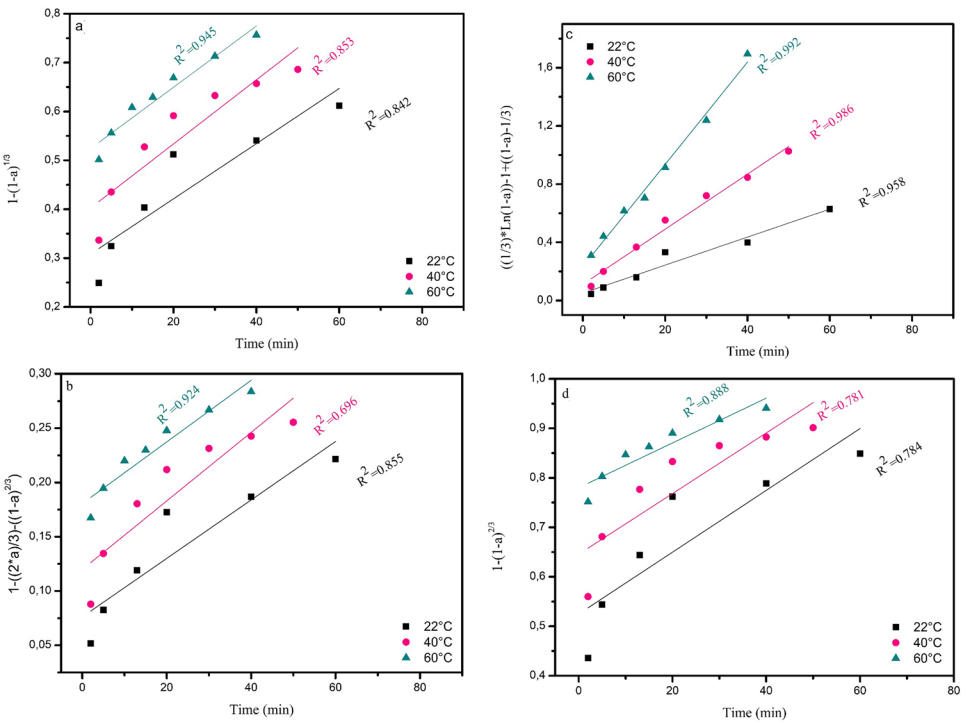

Fig. 5 Kinetic conversion of PG using Na_2CO_3 at different temperatures **a** chemical reaction model, **b** diffusion through the solid layer model, **c** mixed model, and **d** fluid diffusion model

L/S ratio effect

Generally, the variation in the L/S ratio between PG and the conversion solution has an important effect on the conversion efficiency. A series of conversion experiments were carried out with L/S ratios from 7 to 15 using the corresponding stoichiometry of Na_2CO_3, while the other factors are kept constant at T = 22 °C and contact time at 60 min (Fig. 3). The results show that the conversion of PG proportionally increases with L/S in the range of 7–10. The highest value of 97.4% was achieved when the L/S ratio was 10. This could be ascribed to the decrease in diffusion resistance when the L/S ratio is increased. Then, with an increase in the L/S ratio from 10 to 15, the conversion rate was constant at a maximum of 97.4%. Therefore, the greatest L/S ratio of the conversion using Na_2CO_3 is 10. Figure 3 reveals the results when using NH_4HCO_3. Indeed, when the L/S ratio was increased from 7 to 10, the conversion rate rose from 75.3 to 92.9%, respectively. A steady conversion was obtained from 10 to 15. Referring to these results, the L/S ratio of 10 could be considered the optimum.

Contact time effect and kinetics

The effect of contact time on PG conversion was studied in the range of 5 to 120 min keeping 10 as the L/S ratio for Na_2CO_3 (0.6 M) and NH_4HCO_3 (1.2 M) reagents. The results shown in (Fig. 4a) demonstrate that the conversion rate of PG increases with time and reaches a maximum of 95% after 60 min. The results of the conversion of PG using NH_4HCO_3 shown in (Fig. 4b) indicate that the conversion rate gradually increased in the range of 7 to 90 min and no further increase with extended time. Hence, the optimum contact time is 90 min.

The conversion kinetics of PG provide more useful information about the rate-determining stage and the involved

Table 3 Correlation coefficient R^2 and rate constants *Ki* of shrinking-core models used

T°C	Using Na_2CO_3						Using NH_4HCO_3					
	22		40		60		22		34		47	
	R_1	K_1	R_2	K_2	R_3	K_3	R_1	K_1	R_2	K_2	R_3	K_3
M_1	0.84	0.0056	0.85	0.0066	0.94	0.0063	0.96	0.0052	0.89	0.0041	0.95	0.007
M_2	0.85	0.0027	0.69	0.0044	0.92	0.0028	0.98	0.0024	0.89	0.002	0.95	0.0034
M_3	0.95	0.0096	0.98	0.0189	0.99	0.0352	0.96	0.0072	0.98	0.0109	0.99	0.0234
M_4	0.78	0.0063	0.78	0.0061	0.88	0.0045	0.90	0.0063	0.84	0.0038	0.93	0.006

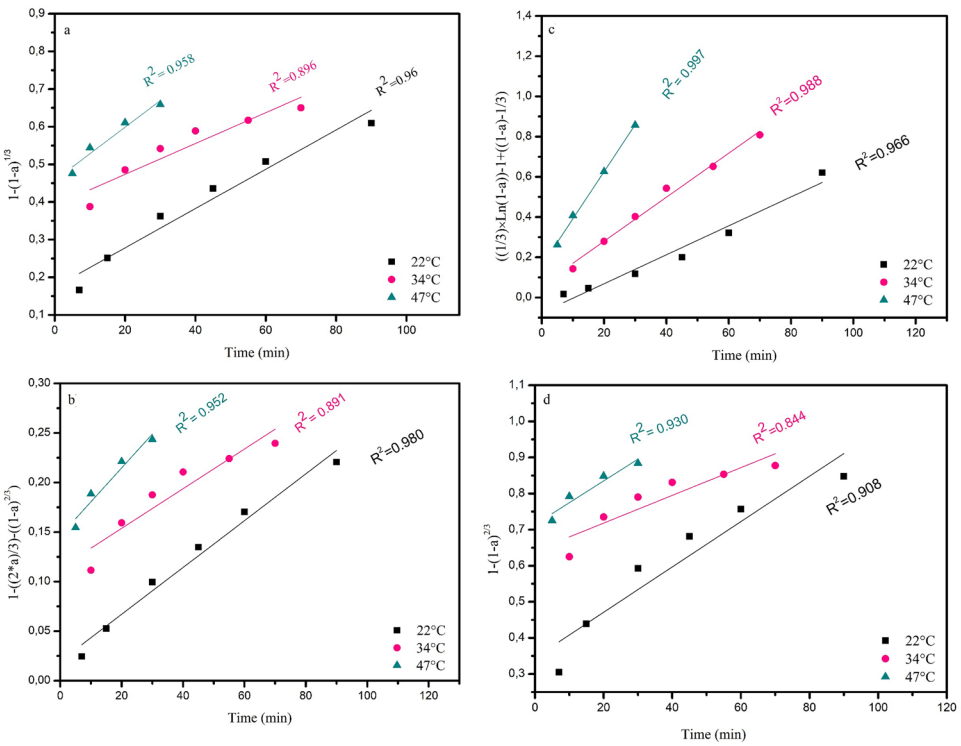

Fig. 6 Kinetic conversion of PG using NH_4HCO_3 at different temperatures **a** chemical reaction model, **b** diffusion through the solid layer model, **c** mixed model, and **d** fluid diffusion model

mechanism. PG conversion is a heterogeneous reaction between ions in the solution and solid particles of PG. For this typical reaction, shrinking-core models (SCMs) are the most common models used to describe the kinetic mechanism that controls the conversion. By applying SCMs, it is possible to identify the slowest step that is considered to be the rate-determining stage. The four models used, including the chemical reaction model [33], diffusion through the solid layer model, mixed model, and fluid diffusion model, are described using Eqs. 4–7, respectively [27]

$$1-(1-\mathrm{X})^{\frac{1}{3}} = K_1 \mathrm{t} \tag{4}$$

$$1-2a/3-(1-\mathrm{X})^{\frac{2}{3}} = K_2 t \tag{5}$$

$$1/3\ln(1-\mathrm{X})-1+(1-\mathrm{X})^{\frac{-1}{3}} = K_3 t \tag{6}$$

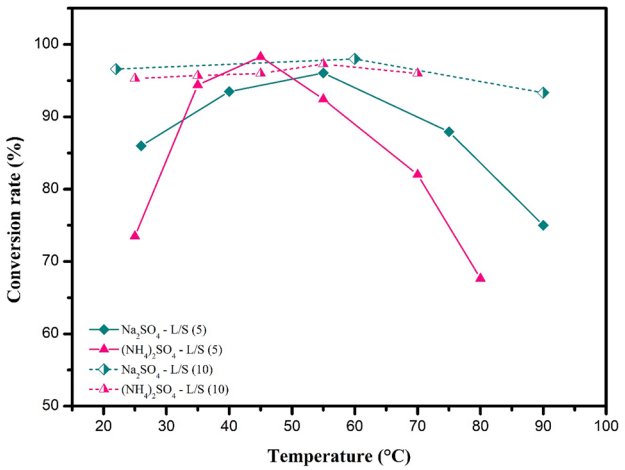

Fig. 7 Effect of temperature on the conversion rate of PG using sodium carbonate and ammonium bicarbonate

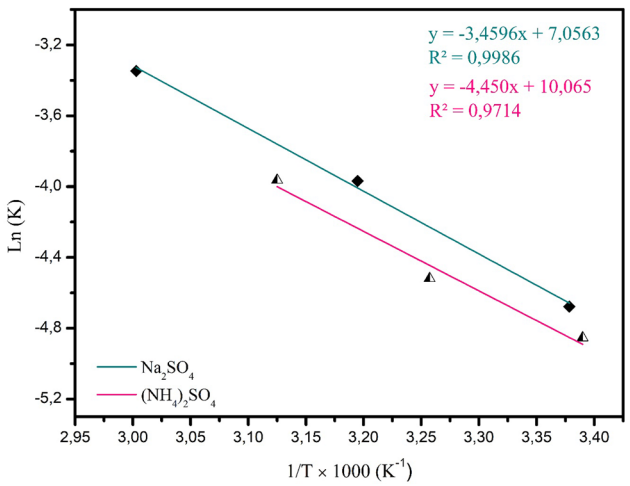

Fig. 8 Arrhenius plot for conversion of PG using sodium carbonate and ammonium bicarbonate

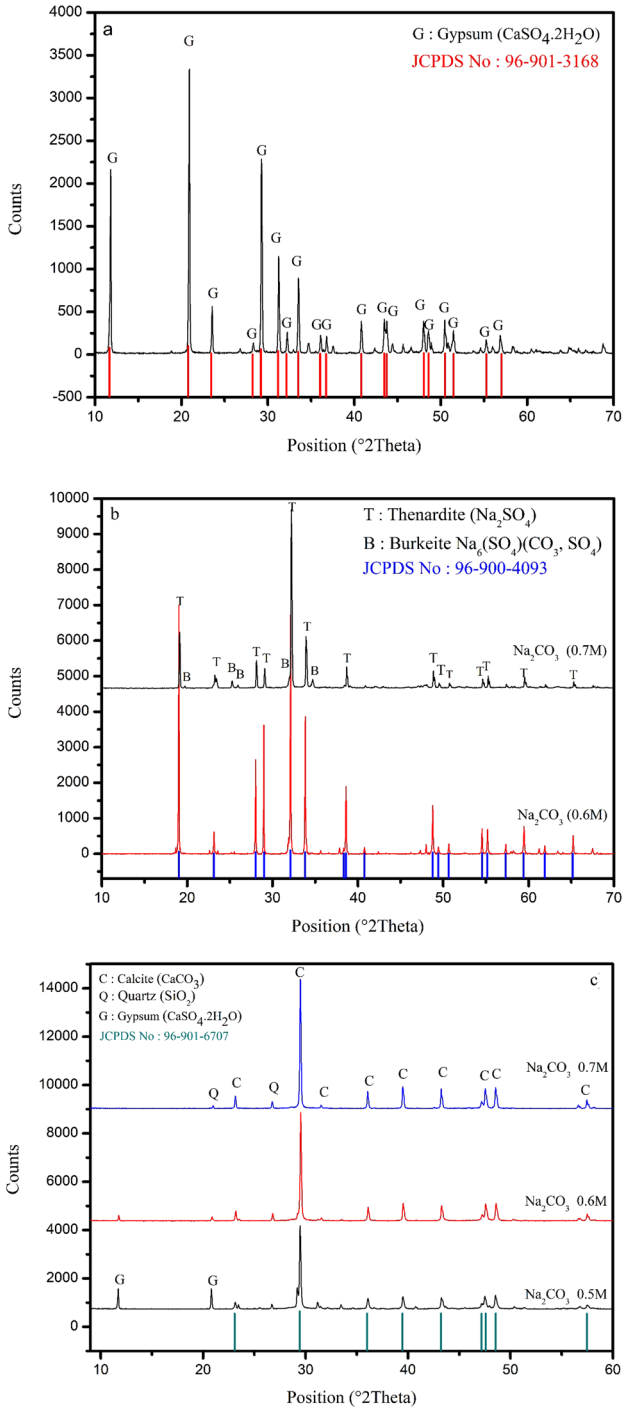

Fig. 9 XRD pattern of **a** PG, **b** crystallized Na_2SO_4, and **c** precipitated $CaCO_3$ at 60 min as contact time

$$1-(1-X)^{\frac{2}{3}} = K_4 t, \quad (7)$$

where X is the PG conversion rate, and K_i is the experimental rate constant that can be calculated according to equations in the study [28]. t is the reaction time. External diffusion was not studied, because the stirring speed used was above 250 rpm. Mashifana et al. reported that with a high stirring speed, external diffusion has no effect on the fractional conversion of PG [29].

Figure 5 represents the four models applied to the conversion using Na_2CO_3. Table 3 lists the associated parameters of SCMs including the correlation coefficients (R^2) and chemical rate constant (ki). The results presented in (Fig. 5c) show a plot of $1/3\ln(1-x)+(1-x)-1/3-1$ vs. time and the correlation coefficients R^2. All correlation coefficients were greater than 0.97 for 22, 40 and 60 °C. Therefore, the best model that fits the experimental results is the mixed model. This means that both interfacial reaction and diffusion through the product layer are the effective rate controlling the mechanism of PG conversion using Na_2CO_3.

Figure 6 displays the kinetic data plotted for SCMs of the conversion using NH_4HCO_3. Figure 6c shows a linear correlation of k_3 and the conversion rate with correlation coefficients (R^2) over 0.96. The proposed mixed model is in good agreement with the experimental data, attesting that the conversion of PG using NH_4HCO_3 is controlled by this model. Therefore, the model (Eq. (6)) can be used to properly describe the conversion process of PG using NH_4HCO_3. The conversion rate is also greatly affected by the size of the phosphogypsum particles. As the PG particle size decreases (similarly as the diffusion pores increase), the particle surface increases, which enhances the contact between the reagents and the PG particles. In addition, this promotes surface reaction and facilitates diffusion through the product layer, which increases the conversion rate.

Temperature effect

The influence of temperature on the conversion of PG was studied in the range of 22 to 90 °C to study the conversion of PG using Na_2CO_3. At room temperature and with an L/S ratio of 10, the conversion reaches 95%. Hence, the L/S ratio was fixed at 5 to investigate the conversion of a high amount of PG at high temperature. From the results shown in (Fig. 7), it is obvious that the conversion of PG increases with temperature up to reach a maximum of 96% at 55 °C. When the temperature was increased, the particles gained more energy; therefore, there was more collision between the reagents [23]. The conversion decreases with increasing temperature from 60 to 90 °C because of the CO_2 released from the solution [34]. The conversion of PG using NH_4HCO_3 increases until it reaches a maximum of 98% at a temperature of 45 °C (Fig. 7). Then, the conversion highly decreased when the temperature was further elevated to more than 45 °C because of the solubility of both CO_2 and NH_3 which decreased as the temperature increased [35, 36].

The Arrhenius law (Eq. (8)) was used to describe the variation in the kinetic reaction as a function of temperature. A plot of the variation of $\ln(K_3)$ as a function of 1/T is illustrated in (Fig. 8) using the apparent rate constant obtained from the mixed model

$$k = A.e^{\frac{-Ea}{RT}} \quad (8)$$

where A is the pre-exponential factor, Ea is the activation energy (J mol^{-1}), R is the universal gas constant (J mol^{-1} K^{-1}), and T is the absolute temperature (K). The activation energy was calculated from (Fig. 8). The Ki value is inversely proportional to the temperature. The graph slope and intercept obtained were 3,4596 and 7,0563, respectively. The activation energy can be obtained by multiplying the slope value by a global gas constant, and the result is 28,4 kJ mol^{-1}. On the other hand, the use of NH_4HCO_3 as a

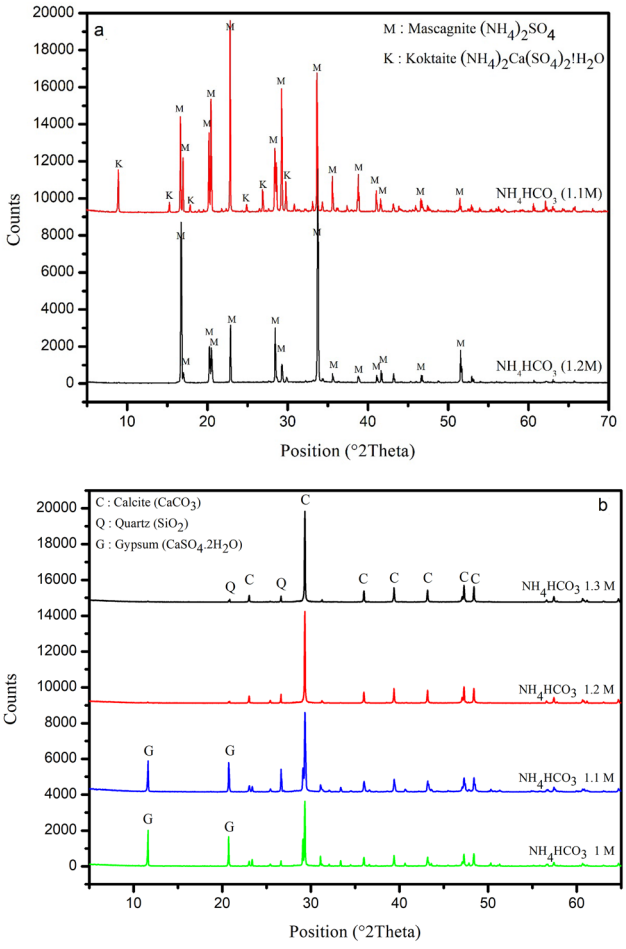

Fig. 10 XRD pattern of **a** crystallized $(NH_4)_2SO_4$, **b** precipitated $CaCO_3$ at 90 min as contact time

reagent leads to an activation energy of 37 kJ mol^{-1} (Fig. 8). These results are in accordance with the mixed model which is usually found to be in the range of 20–42 kJ mol^{-1} [37].

XRD analysis

Figure 9a presents XRD patterns of PG and the obtained products for the conversion process. PG is mainly composed of $CaSO_4.2H_2O$ crystallized in the monoclinic system with space group C12/c1 (96–901-3168 COD, Crystallography Open Database). The precipitate was identified as calcite phase $CaCO_3$ and a trace amount of quartz SiO_2 was detected at 2θ equal to 26.6° (Fig. 9c). The formation of the precipitate can be explained by the reaction between Ca^{2+} and CO_3^{2-} ions Eq. (9). Figures 9c, 10b show that under the optimum conditions for both processes, $CaCO_3$ produced with a calcite phase with a spherical morphology composed of hexagonal blocks (JCPDS 96–901-6707). The product was calcite instead of vaterite because of the time impact on the polymorph of CaCO3. When the reaction time is longer the crystal phase, and the morphology went to calcite due to thermodynamic stability increases in the order of vaterite, aragonite, and calcite. The temperature has the same trend as the time effect and that was confirmed by Chen et al. [25]

$$Ca^{2+}(aq) + CO_3^{2-}(aq) \rightarrow CaCO_3(s) \quad (9)$$

The XRD diffractogram of the salt obtained from the crystallized filtrate (Fig. 9b) indicates that it is mainly crystallized in the form of anhydrous sodium sulfate, Na_2SO_4 (96–900-4093, COD) in an orthorhombic system. Figure 10 shows the scenario in which different concentrations (1, 1.1, 1.2 and 1.3 M) were used to convert PG using NH_4HCO_3. Concentrations below 1.2 M shows signals of gypsum which confirms the partial conversion of PG. The total conversion of PG to Mascagnite (96–900-9883, COD) is evident in Fig. 10a using a concentration of 1.2 M. The formation of undesirable salts is due to the concentration of the reagents, when the reagent is used in insufficient quantity (NH_4HCO_3 1.1 M), the unreacted calcium ions will crystallize in the form of Koktaite. For Burkeite, their formation is due to the excess of the reagent Na_2CO_3 (0.7 M), in the same way the excess of carbonate combines with the sulfate and sodium ions to form Burkeite. These results confirm the optimal conditions of conversion.

FTIR analysis

The phosphogypsum, produced sodium sulfate, and ammonium sulfate were characterized by FTIR (Fig. 11), confirming the structure of the products obtained from the conversion of PG. The FTIR spectrum of PG (Fig. 11a) shows the presence of water molecules. Stretching vibration $\upsilon_{O\text{-}H}$ and bending vibrations $\delta_{O\text{-}H}$ are observed at 3545–3248 and 1686–1621 cm^{-1}, respectively [38]. The vibration located at 2240–2115 and 1143–1113 cm^{-1} is attributed to the

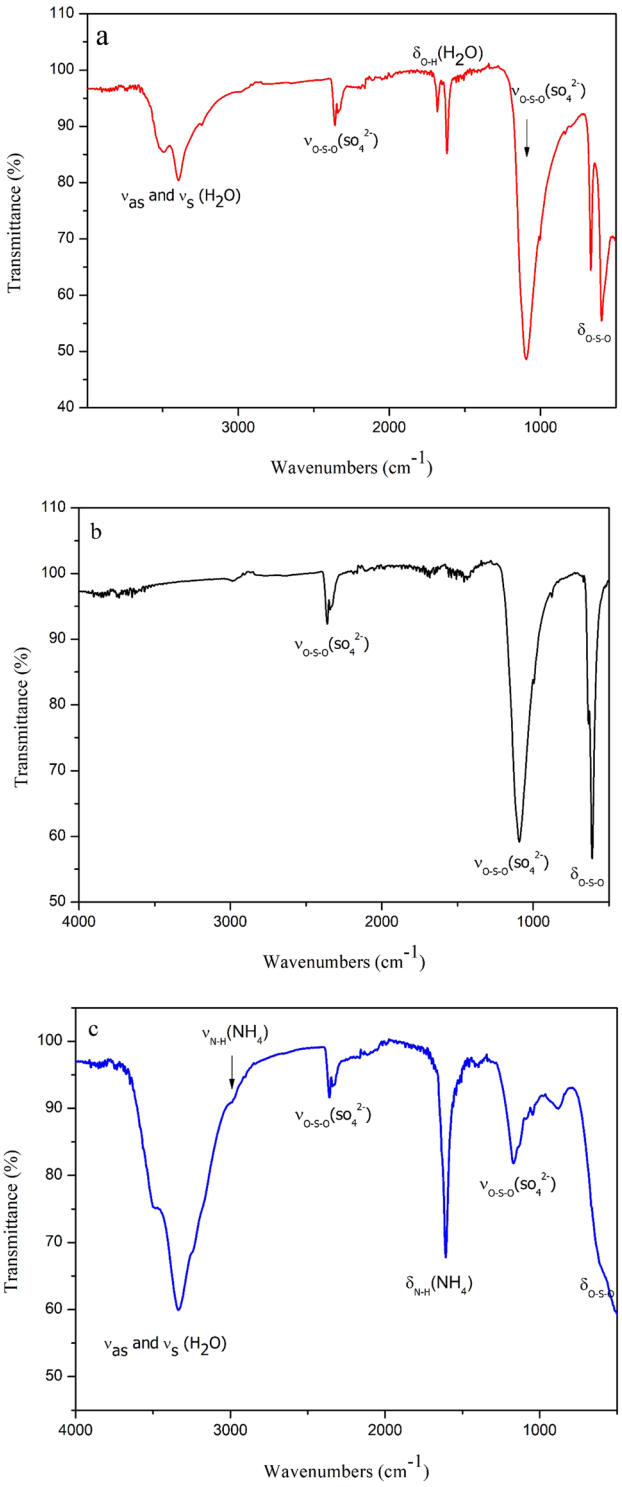

Fig. 11 FTIR spectra of **a** PG, crystallized filtrate derived from PG conversion using **b** sodium carbonate and **c** ammonium bicarbonate

Table 4 Allocation of the infrared vibration of the raw PG and leach filtrates

Vibration type	Wavenumbers (cm^{-1})			
	PG	Sodium sulfate	Ammonium sulfate	
Stretching vibrations $\upsilon_{O\text{-}H}$ of water	3545–3248	–	3493–3331	[38]
Stretching vibrations $\upsilon_{N\text{-}H}$ of ammonium	–	–	2983	[39]
Stretching vibrations $\upsilon_{O\text{-}S\text{-}O}$ of SO_4^{2-}	2240–2115	2361–2338	2360–2337	[15]
Bending vibrations $\delta_{O\text{-}H}$ of water	1686–1621	–	–	[38]
Bending vibrations $\delta_{N\text{-}H}$ of ammonium	–	–	1606	[39]
Stretching vibrations $\upsilon_{O\text{-}S\text{-}O}$ of SO_4^{2-}	1143–1113	1090	1169	[15]
Bending vibrations $\delta_{O\text{-}S\text{-}O}$ of SO_4^{2-}	668–602	631–611	614	[18]

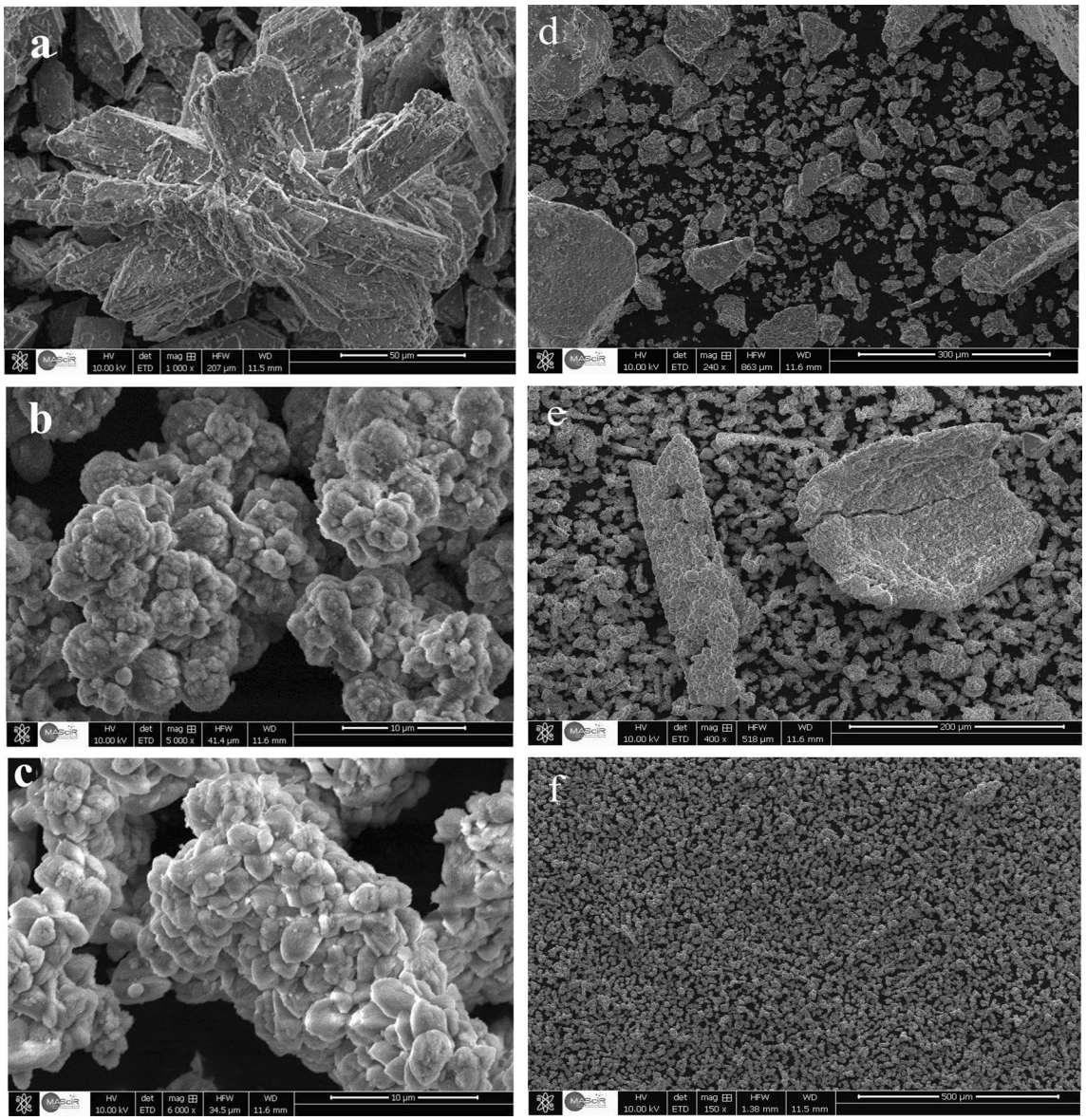

Fig. 12 SEM images of **a** PG, **b** precipitate from the sodium carbonate process, **c** precipitate from the ammonium bicarbonate process, **d** evaporated filtrate of sodium sulfate, precipitated $CaCO_3$ **e** at 30 min and **f** at 60 min

Table 5 Major and trace elements in PG and conversion products

	Unit	PG	WPG	NH_4HCO_3 carbonation		Na_2CO_3 carbonation	
				NH_4SO_4	$CaCO_3$	Na_2SO_4	$CaCO_3$
SO_3	%	44.71	45.8	60.7	1.67	56.1	2.81
CaO	%	32.95	33.4	0.0011	46.26	0.002	46.68
F	%	1.88	0.97	0.07	1.05	0.06	0.94
P_2O_5	%	0.9	0.83	0.90	1.32	0.91	1.02
SiO_2	%	2.66	3.34	–	0.62	0.55	0.55
Al_2O_3	%	0.16	0.1	< 0.0005	0.1933	0.0024	0.1138
Fe_2O_3	%	0.04	0.01	< 0.0005	0.0118	< 0.0005	0.0089
K_2O	%	0.008	0.008	0.0003	0.0196	0.0002	0.0206
MgO	%	0.031	0.022	0.0003	0.0194	< 0.0005	0.0266
Na_2O	%	0.15	0.08	0.0017	0.7446	28.5	1.482
Cd	Ppm	3	1	0.0015	2.992	< 0.0010	2.653
V	Ppm	16	15	< 0.0010	9.205	0.0415	7.275
Cr	Ppm	9.3	9	0.0091	11.6	< 0.0010	8.502

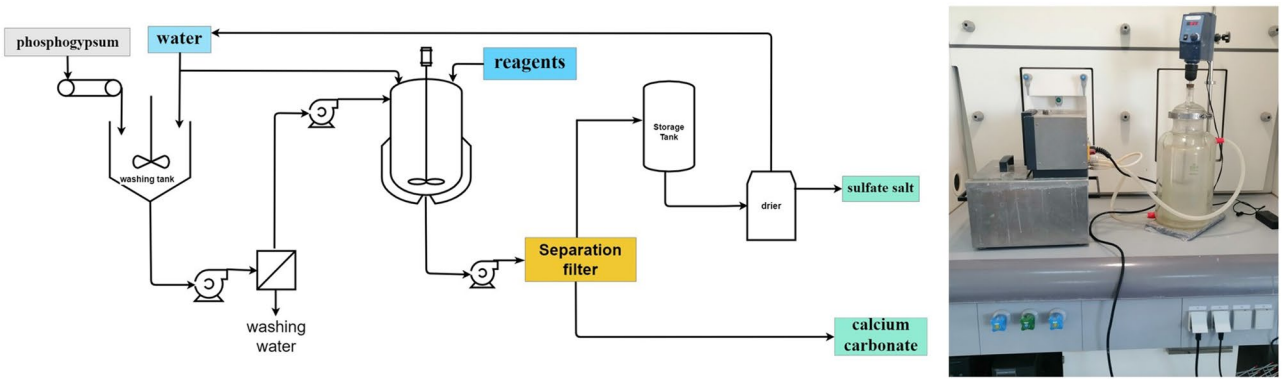

Fig. 13 Flowsheet of the PG conversion process

Table 6 Principal equipment description and cost

Equipment	Capacity	Number	Material costs $	% CI
Conversion reactor, ton	100	2	1,000,000	49.75
Storage tank, ton	10 000	4	200 000	9.95
Filter ton /h	20	3	80 000	3.98
Solid Conveyor ton/h	100	3	50 000	2.49
Pumps m3/h	10	7	80 000	3.98
Piping		–	600 000	29.85
Total CAPEX/20 Years			2 010 000	

stretching vibration $\upsilon_{O\text{-}S\text{–}O}$ of SO_4^{2-}. The bending vibration $\delta_{O\text{-}S\text{–}O}$ is observed at 668–602 cm^{-1} [15]. Figure 11b shows the FTIR spectrum of the crystallized filtrate produced from PG using Na_2CO_3. The results indicate the presence of the strong sulfur–oxygen-stretching vibration $\upsilon_{O\text{-}S\text{–}O}$ of SO_4^{2-} at 1090 cm^{-1} and bending vibration $\delta_{O\text{-}S\text{–}O}$ bands at 631–611 cm^{-1} [18]. The unmarked group of bands near 2200 cm^{-1} are the combination bands of the lower wavenumbers S–O [15, 18]. Moreover, the crystallized FTIR spectrum, displayed in Fig. 11c shows typical N–H vibrations. The bands observed at 2983 and 1606 cm^{-1}, correspond to the $\upsilon_{N\text{-}H}$ stretching band and $\delta_{N\text{-}H}$ deformation band, respectively [39]. In conclusion, the FTIR results (Table 4) are in good agreement with those obtained by XRD analysis.

SEM analysis

Figure 12 illustrates the morphological structure of PG and precipitated calcium carbonate. As seen in Fig. 12a, PG particles have a hexagonal crystal structure. This morphology depends essentially on the composition of PG (impurities, PO_4^{2-} syncrystallized ions), condition of crystallization (nature of the rock, attack process, etc.). In addition, the morphology also depends on the size of these particles in the range of 20–200 µm. As observed by comparing SEM images of PG and precipitated $CaCO_3$ particles,

Table 7 Operating cost of the first process

Input	Unit cost, $	Unit consumption per ton of phosphogypsum	Unit cost per ton of phosphogypsum	Annual cost, $ million
Phosphogypsum, ton	0	1	0	0.00
Sodium carbonate, ton	90	0.57	51.3	9.36
Electricity, kWh	0.05	50	2.5	0.45
Water, ton	0.5	10	5	0.91
Labor				0.3
Maintenance				0.2
Total OPEX				11.22

Table 8 Operating cost of the second process

Input	Unit cost, $	Unit consumption per ton of phosphogypsum	Unit cost per ton of phosphogypsum	Annual cost, $ millions
Phosphogypsum, ton	0	1	0	0.00
Ammonium bicarbonate, ton	135	0.94	126.9	23.16
Electricity, kWh	0.05	50	2.5	0.45
Water, ton	0.5	10	5	0.91
Labor				0.3
Maintenance				0.2
Total OPEX				25.02

Table 9 Determination of revenues

Product	Quality	Quantity produced per ton of phosphogypsum	Market value $	Revenues per ton of phosphogypsum	Annual revenues $
Sodium sulfate	99%	0.75	120–130	93.7	
Calcium carbonate		0.67	10	6.7	
Total revenues				100.4	18 323 000
Total CAPEX					100 500
Total OPEX					11 220 000
Return on investment (ROI)				41.05	7 002 500 (62.41%)
Ammonium sulfate	99%	0.70	140–150	101.5	
Calcium carbonate		0.68	10	6.8	
Total revenues				108.3	19 764 750
Total CAPEX					100 500
Total OPEX					25 020 000
Return on investment (ROI)					5 355 750 (– 21.4%)

the morphology was changed. Figure 12b, c shows an SEM image of $CaCO_3$ particles produced using Na_2CO_3 or NH_4HCO_3. As observed in these images, fine and agglomerated particles are obtained. However, the size of these particles ranges from 1 to 10 µm. In fact, impurities and trace elements contained in PG can modify the morphology and structure of precipitated particles according to Lu et al. [40]. SEM images Fig. 12e, f clearly show that the surface area of the PG particles was significantly affected by the reagent. It is clear from Fig. 12e that the surface area of the particles continues to gradually reduce as the conversion time increases. The fast evolution of the morphology also confirms the dominant effect of the chemical reaction on the particle surface after the diffusion of the reagent through the solid layer, and this is clearly apparent by the formation of the small calcium carbonate particle on the surface of the PG particles. Thus, this also indicates that the leaching kinetics is governed by the mixed controlled shrinkage-core model.

Chemical composition of PG and products of the conversion

Table 5 represents the chemical analysis of the trace elements in the products. During the conversion process, the transfer factor of trace metals into the precipitated $CaCO_3$ is high, approximately 90%. Hence, sodium sulfate and ammonium sulfate were obtained with high purity. Divalent metals such as Pb, Ni, Cu, Cd, and Zn can be easily incorporated into the precipitate because of adsorption on the precipitated particle surface. Moreover, the trapping phenomenon during precipitation is an effective mechanism for reducing metals mobility in aqueous systems, which causes them to be transferred into the precipitate [19]. The conversion of PG using carbonate solutions leads to the obtaining of Na_2SO_4 and $(NH_4)_2SO_4$ products with fewer impurities. These results were also observed by other authors [41].

Economic feasibility

A preliminary analysis of the PG conversion process (Fig. 13) was conducted to investigate the economic viability of an industrial plant. The estimated capital expenditure for a 500 ton/day (180 000 tons/year) of phosphogypsum conversion plant is provided in (Table 6). The operating costs of each conversion process are discussed in Tables 7, 8. According to the process of conversion using sodium carbonate, 1 ton of PG can be treated by 0.57 ton of Na_2CO_3 (51.3$) to obtain 0.67 ton of $CaCO_3$ (6.7 $) and 0.75 ton (93.7 $) of Na_2SO_4. This economic approach yields 7.49 M$ per year, with an ROI up to 69%. The second conversion process requires a high amount (0.94 ton) of ammonium bicarbonate for one ton of PG, which results in a net loss of approximately 31.35 $/ton (Table 9). Based on these results, the first process seems more economically valuable than the second one. This is due to the amount of ammonium bicarbonate needed to convert the totality of PG. Moreover, using ammonium carbonate is more efficient because of the stoichiometry condition of the reaction with $CaSO_4.2H_2O$. From the socioeconomic side, these processes remain environmentally sustainable for the management of PG waste and do not require complicated operation.

Conclusion

In this work, a total conversion of PG using sodium carbonate and ammonium bicarbonate by precipitation of calcium carbonate was confirmed. Conversion kinetics under simulated experimental conditions are discussed, and Shrinking-core models are established. A possible conversion reaction mechanism is also proposed.

The kinetic results for both reactions showed that the conversion of PG was in accordance with the mixed model with equation $1/ln(1-a) - 1 + (1-a)^{\frac{-1}{3}} = K_3 t$, and the conversion reaction mechanism was controlled by the interfacial reaction and diffusion through the product layer. The Ea of PG conversion in Na_2CO_3 was 29.4 kJ mol^{-1}. However, the use of NH_4HCO_3 as a reagent leads to an activation energy of 27.9 kJ mol^{-1}. By comparing the activation energy of these two reactions, it can be determined that the conversion in NH_4HCO_3 is easier than that in Na_2CO_3. The precipitation of calcium does not require more demanding reaction conditions due to the amount of excess CO_3^{2-} ions in the solution.

The economic study was carried out considering the main expenses namely chemicals and energy consumption. Therefore, the economic evaluation of the processes reveals that the conversion using sodium carbonate was economically viable. This is due to the low cost of the sodium carbonate reagents.

Acknowledgements The authors would like to express their gratitude to Mohammed VI polytechnic University and OCP group for their financial support and leadership of the project.

Author contributions All authors contributed to the study conception and design. The first draft of the manuscript was written by KA. All authors commented on previous versions of the manuscript. All authors read and approved the final manuscript.

Funding The authors declare that no funds, grants, or other support were received during the preparation of this manuscript.

Declarations

Conflict of interest The authors have no relevant financial or non-financial interests to disclose.

References

1. Amrani M, Taha Y, Kchikach A et al (2020) Phosphogypsum recycling: new horizons for a more sustainable road material application. J Build Eng 30:101267. https://doi.org/10.1016/j.jobe.2020.101267
2. Bouargane B, Marrouche A, El Issiouy S et al (2019) Recovery of Ca(OH)2, CaCO3, and Na2SO4 from Moroccan phosphogypsum waste. J Mater Cycles Waste Manag 21:1563–1571. https://doi.org/10.1007/s10163-019-00910-9
3. Tayibi H, Choura M, López FA et al (2009) Environmental impact and management of phosphogypsum. J Environ Manage 90:2377–2386. https://doi.org/10.1016/j.jenvman.2009.03.007
4. Ennaciri Y, Bettach M (2018) Procedure to convert phosphogypsum waste into valuable products. Mater Manuf Processes 33:1727–1733. https://doi.org/10.1080/10426914.2018.1476763
5. Ennaciri Y, Bettach M, El Alaoui-Belghiti H (2020) Recovery of nano-calcium fluoride and ammonium bisulphate from phosphogypsum waste. Int J Environ Stud 77:297–306. https://doi.org/10.1080/00207233.2020.1737426
6. Corisco JAG, Mihalík J, Madruga MJ et al (2017) Natural radionuclides, rare earths and heavy metals transferred to the wild

vegetation covering a phosphogypsum stockpile at Barreiro. Portugal Water Air Soil Pollut 228:235. https://doi.org/10.1007/s11270-017-3413-6
7. Borges RC, Ribeiro FCA, da Costa Lauria D et al (2013) Influence of phosphogypsum stacks on the distribution of natural radionuclides in surface and subsurface waters in the city of Imbituba, SC. Brazil. Water Air Soil Pollut 224:1540. https://doi.org/10.1007/s11270-013-1540-2
8. Enamorado S, Abril JM, Mas JL et al (2009) Transfer of Cd, Pb, Ra and U from phosphogypsum amended soils to tomato plants. Water Air Soil Pollut 203:65–77. https://doi.org/10.1007/s11270-009-9992-0
9. Rashad AM (2017) Phosphogypsum as a construction material. J Clean Prod 166:732–743. https://doi.org/10.1016/j.jclepro.2017.08.049
10. Gijbels K, Nguyen H, Kinnunen P et al (2019) Feasibility of incorporating phosphogypsum in ettringite-based binder from ladle slag. J Clean Prod 237:117793. https://doi.org/10.1016/j.jclepro.2019.117793
11. Papastefanou C, Stoulos S, Ioannidou A, Manolopoulou M (2006) The application of phosphogypsum in agriculture and the radiological impact. J Environ Radioact 89:188–198. https://doi.org/10.1016/j.jenvrad.2006.05.005
12. Hammas-Nasri I, Horchani-Naifer K, Férid M, Barca D (2019) Production of a rare earths concentrate after phosphogypsum treatment with dietary NaCl and Na2CO3 solutions. Miner Eng 132:169–174. https://doi.org/10.1016/j.mineng.2018.12.013
13. Benali K, Kounbach S, Boulif R, Benhida R, Khaless K (2022) Development of a simple and fast ultrasound-assisted extraction method for iodine determination in phosphate rock and phosphogypsum by-product using titrimetric method. Int J Environ Anal Chem. https://doi.org/10.1080/03067319.2022.2091931
14. Xue S, Li M, Jiang J et al (2019) Phosphogypsum stabilization of bauxite residue: conversion of its alkaline characteristics. J Environ Sci 77:1–10. https://doi.org/10.1016/j.jes.2018.05.016
15. Hammas I, Horchani-Naifer K, Férid M (2013) Solubility study and valorization of phosphogypsum salt solution. Int J Miner Process 123:87–93. https://doi.org/10.1016/j.minpro.2013.05.008
16. He H, Hao L, Fan C et al (2022) A two-step approach to phosphogypsum decomposition: oxidation of CaS with CO_2. Thermochim Acta 708:179122. https://doi.org/10.1016/j.tca.2021.179122
17. Aagli A, Tamer N, Atbir A et al (2005) Conversion of phosphogypsum to potassium sulfate: part I. The effect of temperature on the solubility of calcium sulfate in concentrated aqueous chloride solutions. J Therm Anal Calorim 82:395–399. https://doi.org/10.1007/s10973-005-0908-y
18. Zemni S, Hajji M, Triki M et al (2018) Study of phosphogypsum transformation into calcium silicate and sodium sulfate and their physicochemical characterization. J Clean Prod 198:874–881. https://doi.org/10.1016/j.jclepro.2018.07.099
19. Cárdenas-Escudero C, Morales-Flórez V, Pérez-López R et al (2011) Procedure to use phosphogypsum industrial waste for mineral CO_2 sequestration. J Hazard Mater 196:431–435. https://doi.org/10.1016/j.jhazmat.2011.09.039
20. Mattila H-P, Zevenhoven R (2015) Mineral carbonation of phosphogypsum waste for production of useful carbonate and sulfate salts. Front Energy Res. https://doi.org/10.3389/fenrg.2015.00048
21. Msila X, Billing DG, Barnard W (2016) Capture and storage of CO_2 into waste phosphogypsum: the modified Merseburg process. Clean Techn Environ Policy 18:2709–2715. https://doi.org/10.1007/s10098-016-1157-4
22. Danielik V, Fellner P, Jurišová J, Králik M (2018) Kinetics of the conversion reaction of gypsum with ammonium carbonate. Chem Pap 72:2631–2639. https://doi.org/10.1007/s11696-018-0493-8
23. Kandil A-HT, Cheira MF, Gado HS et al (2017) Ammonium sulfate preparation from phosphogypsum waste. J Radiat Res Appl Sci 10:24–33. https://doi.org/10.1016/j.jrras.2016.11.001
24. Mulopo J, Omoregbe DI (2012) Phosphogypsum conversion to calcium carbonate and utilization for remediation of acid mine drainage. J Chem Eng Process Technol. https://doi.org/10.4172/2157-7048.1000129
25. Chen Q, Ding W, Sun H et al (2020) Utilization of phosphogypsum to prepare high-purity $CaCO_3$ in the NH_4Cl–NH_4OH–CO_2 system. ACS Sustainable Chem Eng 8:11649–11657. https://doi.org/10.1021/acssuschemeng.0c03070
26. Zdah I, El Alaoui-Belghiti H, Cherrat A et al (2021) Temperature effect on phosphogypsum conversion into potassium fertilizer K2SO4 and portlandite. Nanotechnol Environ Eng 6:27. https://doi.org/10.1007/s41204-021-00122-3
27. Ait Brahim J, Ait Hak S, Achiou B et al (2022) Kinetics and mechanisms of leaching of rare earth elements from secondary resources. Miner Eng 177:107351. https://doi.org/10.1016/j.mineng.2021.107351
28. Islas H, Flores MU, Reyes IA et al (2020) Determination of the dissolution rate of hazardous jarosites in different conditions using the shrinking core kinetic model. J Hazard Mater 386:121664. https://doi.org/10.1016/j.jhazmat.2019.121664
29. Mashifana T, Ntuli F, Okonta F (2019) Leaching kinetics on the removal of phosphorus from waste phosphogypsum by application of shrinking core model. S Afr J Chem Eng 27:1–6. https://doi.org/10.1016/j.sajce.2018.11.001
30. Liu Y, Zhang Q, Chen Q et al (2019) Utilisation of water-washing pre-treated phosphogypsum for cemented paste backfill. Minerals 9:175. https://doi.org/10.3390/min9030175
31. Ennaciri Y, Zdah I, El Alaoui-Belghiti H, Bettach M (2020) Characterization and purification of waste phosphogypsum to make it suitable for use in the plaster and the cement industry. Chem Eng Commun 207:382–392. https://doi.org/10.1080/00986445.2019.1599865
32. Moreira RH, Queiroga FS, Paiva HA et al (2018) Extraction of natural radionuclides in TENORM waste phosphogypsum. J Environ Chem Eng 6:6664–6668. https://doi.org/10.1016/j.jece.2018.10.019
33. Elkanzi EM, Chalabi MF (1991) Kinetics of the conversion of calcium sulfate to ammonium sulfate using ammonium carbonate aqueous solution. Ind Eng Chem Res 30:1289–1293. https://doi.org/10.1021/ie00054a032
34. Liu Y, Hou M, Yang G, Han B (2011) Solubility of CO_2 in aqueous solutions of NaCl, KCl, $CaCl_2$ and their mixed salts at different temperatures and pressures. J Supercrit Fluids 56:125–129. https://doi.org/10.1016/j.supflu.2010.12.003
35. Nowak P, Skrzypek J (1989) The kinetics of chemical decomposition of ammonium bicarbonate and carbonate in aqueous solutions. Chem Eng Sci 44:2375. https://doi.org/10.1016/0009-2509(89)85170-X
36. Kolliopoulos G, Papangelakis VG (2019) Temperature and pressure effects on the separation efficiency and desorption kinetics in the NH_3–CO_2–H_2O system. Ind Eng Chem Res 58:12247–12252. https://doi.org/10.1021/acs.iecr.9b01699
37. Kumari A, Sinha MK, Pramanik S, Sahu SK (2018) Recovery of rare earths from spent NdFeB magnets of wind turbine: leaching and kinetic aspects. Waste Manage 75:486–498. https://doi.org/10.1016/j.wasman.2018.01.033
38. Bouargane B, Biyoune MG, Mabrouk A et al (2020) Experimental investigation of the effects of synthesis parameters on the precipitation of calcium carbonate and portlandite from moroccan phosphogypsum and pure gypsum using carbonation route. Waste Biomass Valor 11:6953–6965. https://doi.org/10.1007/s12649-019-00923-3

39. Hammas-Nasri I, Elgharbi S, Ferhi M et al (2020) Investigation of phosphogypsum valorization by the integration of the Merseburg method. New J Chem 44:8010–8017. https://doi.org/10.1039/D0NJ00387E
40. Lu SQ, Lan PQ, Wu SF (2016) Preparation of nano $CaCO_3$ from phosphogypsum by gas–liquid–solid reaction for CO_2 sorption. Ind Eng Chem Res 55:10172–10177. https://doi.org/10.1021/acs.iecr.6b02551
41. Contreras M, Pérez-López R, Gázquez MJ et al (2015) Fractionation and fluxes of metals and radionuclides during the recycling process of phosphogypsum wastes applied to mineral CO2 sequestration. Waste Manage 45:412–419. https://doi.org/10.1016/j.wasman.2015.06.046

Publisher's Note Springer Nature remains neutral with regard to jurisdictional claims in published maps and institutional affiliations.

Authors and Affiliations

Khalid Agayr[1,2] · Hamza Chanouri[1,2] · Brahim Achiou[3] · Rachid Benhida[1,2] · Khaoula Khaless[1]

Khalid Agayr
khalid.agayr@um6p.ma

[1] Department of Chemical and Biochemical Sciences, Green Process Engineering (CBS.GPE). Mohammed VI Polytechnic University, 43150 Ben Guerir, Morocco

[2] Institut de Chimie de Nice, UMR CNRS 7272, Université Côte d'Azur, 06108 Nice, France

[3] Laboratory of Materials, Membranes and Environment, Faculty of Sciences and Technologies of Mohammedia, Hassan II University of Casablanca, Mohammedia, Morocco